



# A new family of barium-doped $\text{Sr}_{2-x}\text{Ba}_x\text{Fe}_{1.5}\text{Mo}_{0.5}\text{O}_{6-\delta}$ perovskites for application in intermediate temperature solid oxide fuel cells



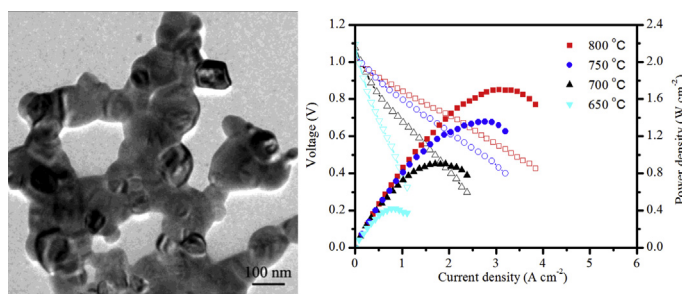
Ningning Dai, Zhenhua Wang, Taizhi Jiang, Jie Feng, Wang Sun, Jinshuo Qiao\*, David Rooney, Kening Sun\*

School of Chemical Engineering and Environment, Beijing Institute of Technology, Beijing, 100081, China

## HIGHLIGHTS

- A novel material  $\text{Sr}_{2-x}\text{Ba}_x\text{Fe}_{1.5}\text{Mo}_{0.5}\text{O}_{6-\delta}$  ( $x = 0, 0.2, 0.4, 0.6, 0.8, 1$ ) were prepared for IT-SOFCs cathodes.
- Investigation on structure and properties of perovskite SBFM materials.
- $\text{SB}_{0.2}\text{FM}$  shows the lowest interface polarization in these cathodes.
- The peak power densities reach 0.87,  $1.30 \text{ W cm}^{-2}$  at 700, 750 °C.

## GRAPHICAL ABSTRACT



## ARTICLE INFO

### Article history:

Received 15 April 2014

Received in revised form

30 May 2014

Accepted 31 May 2014

Available online 9 June 2014

### Keywords:

Solid oxide fuel cell

Element substitution

Cathode

Electrochemical performance

## ABSTRACT

$\text{Sr}_{2-x}\text{Ba}_x\text{Fe}_{1.5}\text{Mo}_{0.5}\text{O}_{6-\delta}$  ( $x = 0, 0.2, 0.4, 0.6, 0.8, 1$ ) perovskite materials have been prepared as potential cathodes for intermediate temperature solid oxide fuel cells (IT-SOFCs) via a sol–gel combustion method. X-ray diffraction (XRD) confirms that the expansion of the unit cell derived from the substitution of the large radius Ba atom, with the impurity phase structure only being detected when  $x = 0.8$  and 1. Concurrently, thermal expansion coefficients (TECs) increase with increasing Ba doping. X-ray photoelectron spectrometry (XPS) measurements show that A-site doped Ba in the perovskite has an insignificant impact on the existence and ratio of  $\text{Fe}^{2+}/\text{Fe}^{3+}$  and  $\text{Mo}^{6+}/\text{Mo}^{5+}$  species within the  $\text{Sr}_{2-x}\text{Ba}_x\text{Fe}_{1.5}\text{Mo}_{0.5}\text{O}_{6-\delta}$  ( $x = 0.2, 0.4, 0.6$ ) (SBFM) samples. Compared with  $\text{Sr}_2\text{Fe}_{1.5}\text{Mo}_{0.5}\text{O}_{6-\delta}$ , the SBFM cathodes exhibited better electrochemical performance, which has been confirmed by the electrochemical impedance spectra (EIS). In particular,  $\text{Sr}_{1.8}\text{Ba}_{0.2}\text{Fe}_{1.5}\text{Mo}_{0.5}\text{O}_{6-\delta}$  ( $\text{SB}_{0.2}\text{FM}$ ) shows the lowest interface polarization ( $R_p$ ). Furthermore the peak power densities of single cells based on the  $\text{SB}_{0.2}\text{FM}$  cathode are 0.87 and  $1.30 \text{ W cm}^{-2}$  at 700 and 750 °C, respectively. All these results suggest that SBFM materials are promising cathodes for IT-SOFCs.

© 2014 Published by Elsevier B.V.

## 1. Introduction

Advanced energy conversion systems such as solid oxide fuel cells (SOFCs) have attracted significant attention due to their high

energy conversion efficiency, fuel flexibility and low pollutant emission [1–3]. To make SOFCs more economically competitive relative to other alternative technologies, it is necessary to develop systems which operate in the intermediate temperature range. These intermediate-temperature solid-oxide fuel cells (IT-SOFCs) have operating temperature between 600 and 800 °C [4–7]. However, the reduction of the operating temperature inhibits the diffusion of oxygen and consequently increases the polarization

\* Corresponding authors. Tel./fax: +86 010 6891 8696.

E-mail addresses: [bitkeninghit@126.com](mailto:bitkeninghit@126.com), [bitkeningsun@163.com](mailto:bitkeningsun@163.com) (K. Sun).

resistance. It is known that this effect is more pronounced at the cathode where the oxygen reduction reaction (ORR) occurs [8,9]. Therefore significant effort has been devoted to exploring new cathode materials for such IT-SOFCs.

The mixed ionic-electronic conductors (MIECs) have been widely studied as alternative cathodes for IT-SOFCs. Most state-of-the-art MIEC materials are classified as perovskite-oxides, ABO<sub>3</sub>-type mixed metal oxides. Recently a new perovskite electrode material, Sr<sub>2</sub>Fe<sub>1.5</sub>Mo<sub>0.5</sub>O<sub>6-δ</sub> (SFM), has attracted much attention since it can be used as both the cathode and anode for SOFCs in a symmetrical configuration owing to its good redox stability and catalytic activity in both oxidizing and reducing environments [10–12]. Generally, partially or full substitution of A and/or B site elements is an effective way to modify the perovskite-type materials in order to improve performance. Hitherto Sr<sub>2</sub>Fe<sub>1.5-x</sub>Co<sub>x</sub>Mo<sub>0.5</sub>O<sub>6-δ</sub> (SFCM) and Sr<sub>2</sub>Fe<sub>1.5-x</sub>Ni<sub>x</sub>Mo<sub>0.5</sub>O<sub>6-δ</sub> (SFNM) materials have been reported [13,14]. Both studies have demonstrated that partial B-site substitution with transition-metal elements enhanced the conductivity and electrochemical performance, with the suggestion that this derived from the impact on the cation valence and oxygen-vacancy concentration in these materials.

Compared with B-site doping, A-site doping is a different strategy to tailor the chemical and physical properties. However, there are no current reports on the effect of A-site doping on the properties and performance of SFM materials. Generally the presence of Ba, with its large ionic radius (1.60 Å), is considered beneficial to induce a large lattice spacing, higher mobility of oxygen ions, and enhanced oxygen reduction reaction rates in perovskite materials [15]. Therefore in present work we investigated the effect of Ba doping at the A-site on the properties of the Sr<sub>2-x</sub>Ba<sub>x</sub>Fe<sub>1.5</sub>Mo<sub>0.5</sub>O<sub>6-δ</sub> system. These Sr<sub>2-x</sub>Ba<sub>x</sub>Fe<sub>1.5</sub>Mo<sub>0.5</sub>O<sub>6-δ</sub> ( $x = 0, 0.2, 0.4, 0.6, 0.8, 1$ ) materials were prepared using a sol-gel combustion method. For the composition of  $x = 0.8$  and 1, a second impurity phase was observed in addition to the perovskite phase. Therefore, the pure Sr<sub>2-x</sub>Ba<sub>x</sub>Fe<sub>1.5</sub>Mo<sub>0.5</sub>O<sub>6-δ</sub> ( $x = 0.2, 0.4, 0.6$ ) perovskite (hereafter abbreviated as SBFM) were systematically investigated in terms of crystal structure, thermal expansion, chemical compatibility with electrolytes and element valence. In addition, the performance of the materials as IT-SOFC cathodes was also examined.

## 2. Experimental

### 2.1. Materials preparation and characterization

Perovskite SBFM samples were synthesized via a sol-gel combustion method. Stoichiometric amounts of Sr(NO<sub>3</sub>)<sub>2</sub>, Ba(NO<sub>3</sub>)<sub>2</sub>, Fe(NO<sub>3</sub>)<sub>3</sub>·9H<sub>2</sub>O, (NH<sub>4</sub>)<sub>6</sub>Mo<sub>7</sub>O<sub>24</sub>·4H<sub>2</sub>O, were used as the metal precursors. Glycine and Citric acid were used to assist combustion. The as-prepared ash was then calcined at 1000 °C for 5 h in air to obtain SBFM powders. The detailed synthesis process can be found in our previous work [16,17]. Four to five drops of poly (vinyl alcohol) (PVA) were then added into the as-synthesized powders (1 g), and ground for about 5 min. Then resulting powder was then pressed into rectangular bars of 25 mm × 5 mm × 5 mm under a pressure of 300 MPa, followed by sintering at 1200 °C for 5 h for subsequent thermal expansion coefficient (TEC) tests and conductivity measurements. The materials also used in this work included La<sub>0.9</sub>Sr<sub>0.1</sub>Ga<sub>0.8</sub>Mg<sub>0.2</sub>O<sub>3</sub> (LSGM) (Fuel cell materials Co., USA), Sm<sub>0.2</sub>Ce<sub>0.8</sub>O<sub>1.95</sub> (SDC) (Fuel cell materials Co., USA), 8%Y<sub>2</sub>O<sub>3</sub>-stabilized ZrO<sub>2</sub> (YSZ, Tosoh Co., Japan) and NiO (High Purity Chemicals, Japan).

The crystal structure of the SBFM materials was determined by X-ray diffraction (XRD) (X' Pert PRO MPD). The microstructure of

the powders was observed using a scanning electron microscope (SEM, FEI QUANTA-250) and transmission electron microscopy (TEM, FEI TECNAI F20). The TEC was measured using a dilatometer (Netsch DIL 402C) from 40 °C to 1000 °C. The element surface analysis was performed on an X-ray photoelectron spectrometer (XPS, MULTILAB2000, VG). Conductivity measurements were performed using a DC four-probe method on a Keithley 2400 source meter.

### 2.2. Fabrication and electrochemical testing of SBFM cathodes

The three-electrode cells were assembled in order to measure the electrochemical impedance spectra (EIS) for the SBFM cathodes [18]. YSZ electrolytes were made by pressing discs (15 mm diameter × 0.8 mm thickness) which were fired at 1500 °C for 6 h. The SDC interlayer was screen-printed onto a YSZ electrolyte and then sintered at 1400 °C for 6 h. The obtained SDC interlayer was approximately 4 μm thick. The SBFM working electrode (WE) with

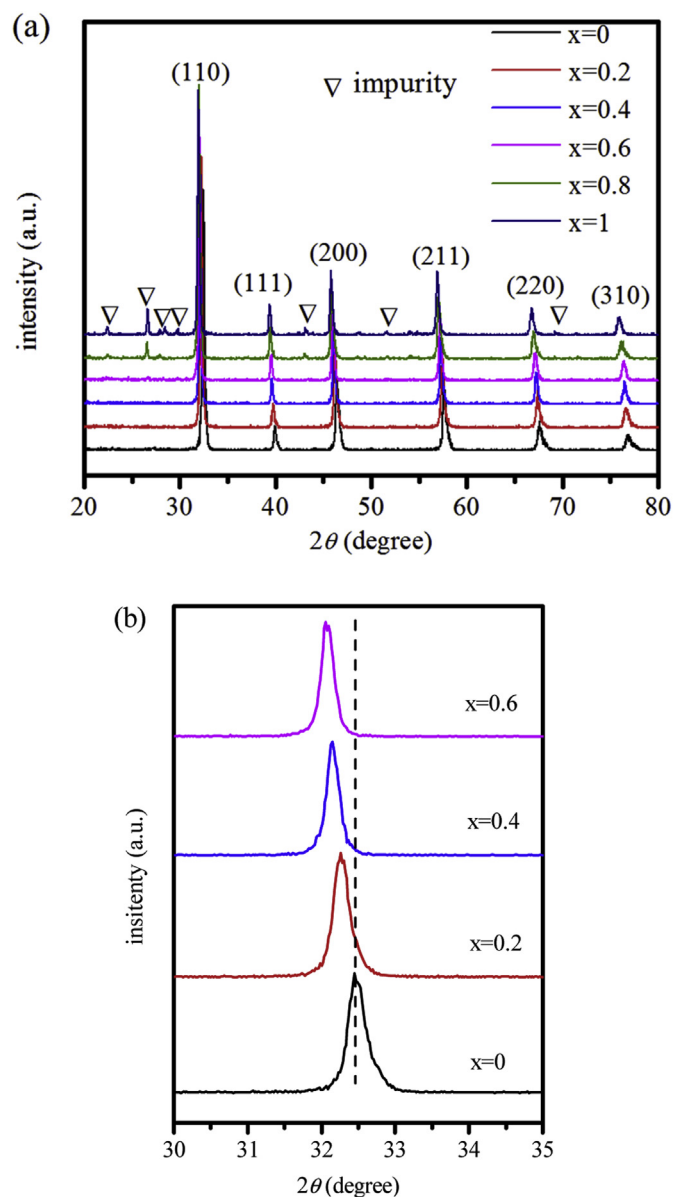


Fig. 1. XRD patterns of Sr<sub>2-x</sub>Ba<sub>x</sub>Fe<sub>1.5</sub>Mo<sub>0.5</sub>O<sub>6-δ</sub> ( $x = 0, 0.2, 0.4, 0.6, 0.8, 1$ ) powders after calcination at 1000 °C in air for 5 h (a)  $2\theta$  from 20 to 80°, (b)  $2\theta$  from 30° to 35°.

**Table 1**The lattice constant of  $\text{Sr}_{2-x}\text{Ba}_x\text{Fe}_{1.5}\text{Mo}_{0.5}\text{O}_{6-\delta}$  ( $x = 0, 0.2, 0.4, 0.6$ ) oxides.

Samples	$a$ b c/Å	Volume/Å <sup>3</sup>	Density/g cm <sup>-3</sup>
$x = 0$	3.9266	60.54	5.8018
$x = 0.2$	3.9347	60.92	6.7870
$x = 0.4$	3.9427	61.29	6.7751
$x = 0.6$	3.9672	62.44	5.6257

an area of 0.25 cm<sup>2</sup> was screen-printed onto the SDC interlayer, and then sintered at 1000 °C for 2 h in air. A Pt reference electrode (RE) was attached on the same side as the WE, and was about 4 mm away from the WE. Pt paste was painted symmetrically on the other side of YSZ electrolyte as the counter electrode (CE). The cell was fired 850 °C for 0.5 h before EIS testing. A PARSTAT 2273 was used to measure the EIS for the SBFM cathodes, with the frequency ranging from 10 mHz to 100 kHz and the AC amplitude of 10 mV under an air atmosphere.

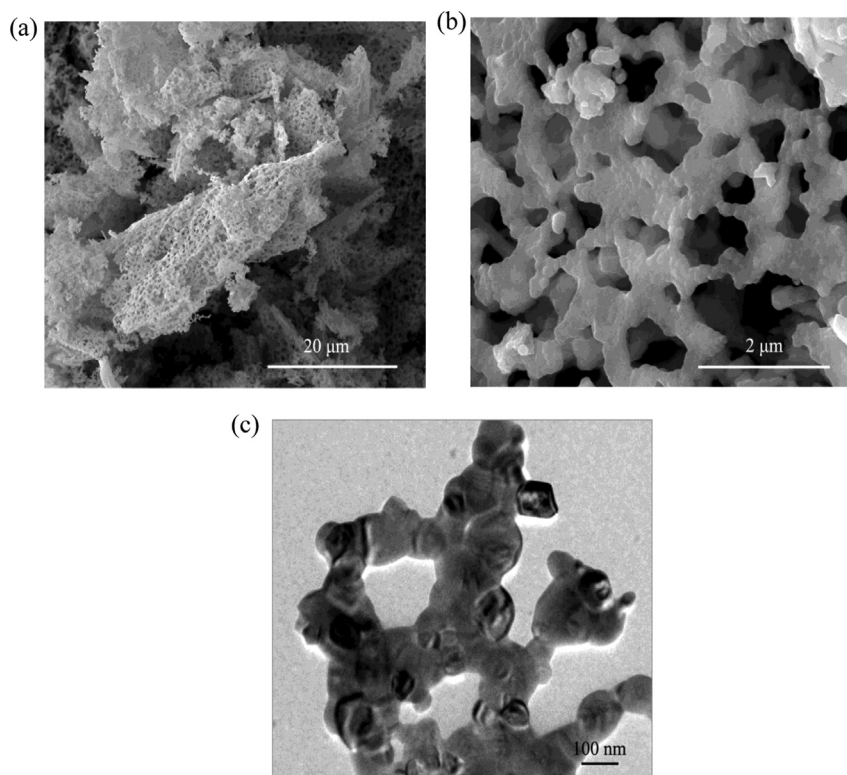
The performance of the SBFM cathodes was studied by assembling single cells. NiO-YSZ anode supported cells with a YSZ electrolyte film were prepared by co-tape casting technology [19]. The thickness of the anode and the electrolyte film produced by this method was approximately 700 μm and 10 μm, respectively. The SDC interlayer was approximately 4 μm thick. The SBFM cathodes were then screen-printed onto the SDC interlayer, and calcined at 1000 °C for 2 h to obtain the NiO-YSZ/YSZ/SDC/SBFM single cells. The cathode area was about 0.25 cm<sup>2</sup> and the thickness was about 10 μm. The single cells were sealed on an alumina tube using silver paste conductive adhesive. The Ag paste was used as a current collector for the cathode. Ag wire was used as a current lead and was connected to the electrodes using Ag paste. The cells were tested with humidified hydrogen (3 vol% H<sub>2</sub>O) as the fuel at a flow rate of 50 mL min<sup>-1</sup> and with ambient air as the oxidant. The current–voltage curves of the cells were recorded on an Arbin instruments tester (Fuel Cell Test System, FCTS).

### 3. Results and discussion

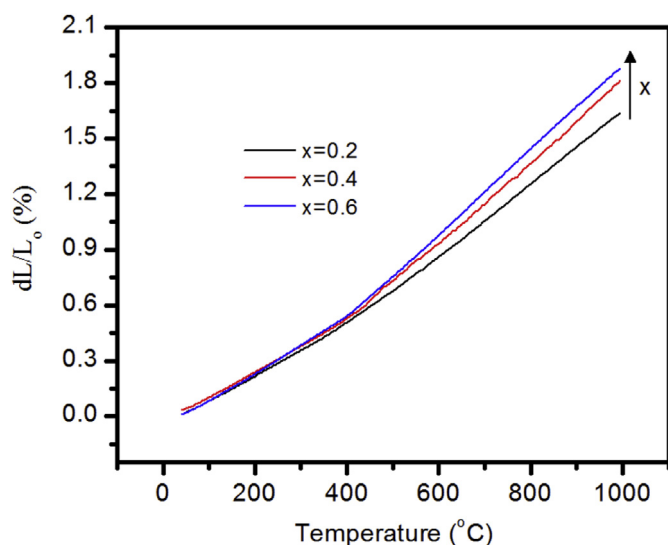
#### 3.1. Crystal structure and microstructure

Fig. 1(a) shows the XRD patterns of  $\text{Sr}_{2-x}\text{Ba}_x\text{Fe}_{1.5}\text{Mo}_{0.5}\text{O}_{6-\delta}$  ( $x = 0, 0.2, 0.4, 0.6, 0.8, 1$ ) powders measured at room temperature. It can be seen that the samples with Ba fractions from 0.2 to 0.6 display a clearly defined perovskite single-phase, and no impurity phase was detected, which implies that partial substitution of Ba for Sr does not affect the formation of a cubic perovskite phase. However, impure phases  $\text{SrMoO}_4$  and  $\text{BaO}$  could be observed in the samples when the Ba-doping concentration was further increased ( $x = 0.8$  and 1). Therefore, in the following work,  $\text{Sr}_{2-x}\text{Ba}_x\text{Fe}_{1.5}\text{Mo}_{0.5}\text{O}_{6-\delta}$  ( $x = 0.2, 0.4, 0.6$ ) (SBFM) samples were systematically studied as cathodes for IT-SOFCs. For more precise evaluation of the effect of Ba substitution at the A-site, the XRD patterns of SBFM materials at ca. 32.4° were magnified and compared, as shown in Fig. 1(b). The peak obviously shifts towards a lower angle since the ionic radius of  $\text{Ba}^{2+}$  (1.60 Å) is larger than  $\text{Sr}^{2+}$  (1.18 Å). As summarized in Table 1, the unit cell parameters increase with increasing Ba content, leading to an increase of unit cell volume. These results indicated that Ba doping at the A-site results in the expansion of the lattice spacing which could facilitate oxygen ionic movement in the perovskite material.

All the prepared SBFM powders produced here have a similar microstructure. Fig. 2 displays the typical microstructure for the  $\text{Sr}_{1.8}\text{Ba}_{0.2}\text{Fe}_{1.5}\text{Mo}_{0.5}\text{O}_{6-\delta}$  ( $\text{SB}_{0.2}\text{FM}$ ) powders sintered at 1000 °C for 5 h. Fig. 2(a) and (b) reveal that the interconnected porous structure is composed of nanoparticles. The average diameter of these pores is approximately 1 μm. The size range of SBFM particles is from 80 to 120 nm, which is confirmed by TEM (Fig. 2(c)). All images indicate that the microstructure of SBFM powders is composed of foam-like interconnected porous tunnels i.e. they are constructed of pores and nanoparticles.



**Fig. 2.** Microstructure of foam-like interconnected porous  $\text{SB}_{0.2}\text{FM}$  powders (a) a low magnification SEM overview, (b) a high magnification SEM image, (c) a TEM image.



**Fig. 3.** Thermal expansion curves of the SBFM samples between 40 °C and 1000 °C in air.

### 3.2. Thermal expansion coefficient and chemical compatibility

The thermal expansion coefficient (TEC) is an important parameter for electrode materials because mismatched TECs in different parts of the cell lead to internal stress and greater likelihood of cracks forming during long-term operation. The thermal expansion curves and TECs obtained for each oxide in the different temperature ranges are displayed in Fig. 3 and Table 2. As shown in Fig. 3, the dilatometric analysis shows a nonlinear behavior at 35–500 °C, which is probably related to the loss of the lattice oxygen in this temperature range in the  $dL/L$  curves [20]. Table 2 lists the TECs of SBFM samples in different temperature ranges. Comparing these TEC values, we can see that the substitution of Ba has affected the TECs of the SBFM materials. The average TEC values increase from  $15.7 \times 10^{-6} \text{ K}^{-1}$  to  $18.1 \times 10^{-6} \text{ K}^{-1}$  with increasing  $x$  (from 0.2 to 0.6) over the temperature range of 40–1000 °C. The TECs of SBFM samples are slightly higher than that of typical electrolytes such as YSZ ( $10.8 \times 10^{-6} \text{ K}^{-1}$ ) [21]. Clearly the SDC ( $12.8 \times 10^{-6} \text{ K}^{-1}$ ) interlayer can adjust to the difference of TECs between SBFM and YSZ materials and thus improve the adhesion between the YSZ electrolyte and SBFM electrode [22].

The chemical compatibility of SBFM powders with the typical electrolyte materials at SOFC operation temperature has been investigated. A mixture of  $\text{SB}_{0.2}\text{FM}$  combined with YSZ, SDC and LSGM powders (50 wt% of each) was milled and then calcined in air at 800 °C for 48 h Fig. 4(a)–(c) shows that no impurity phase was formed with no obvious peak shifting for each component indicating no solid–state reaction between SBFM and YSZ, SDC and LSGM electrolyte materials.

### 3.3. X-ray photoelectron spectroscopy analysis

XPS spectroscopy is widely used to characterize the chemical state and surface properties of materials. Fig. 5 shows the Ba 3d, Fe

**Table 2**

The TECs for SBFM samples between 40 °C and 1000 °C in air.

Samples	TEC ( $\times 10^{-6} \text{ K}^{-1}$ )		
	40–350 °C	500–1000 °C	40–1000 °C
$x = 0.2$	13.4	20.7	15.7
$x = 0.4$	13.5	21.8	16.8
$x = 0.6$	14.3	22.9	18.1

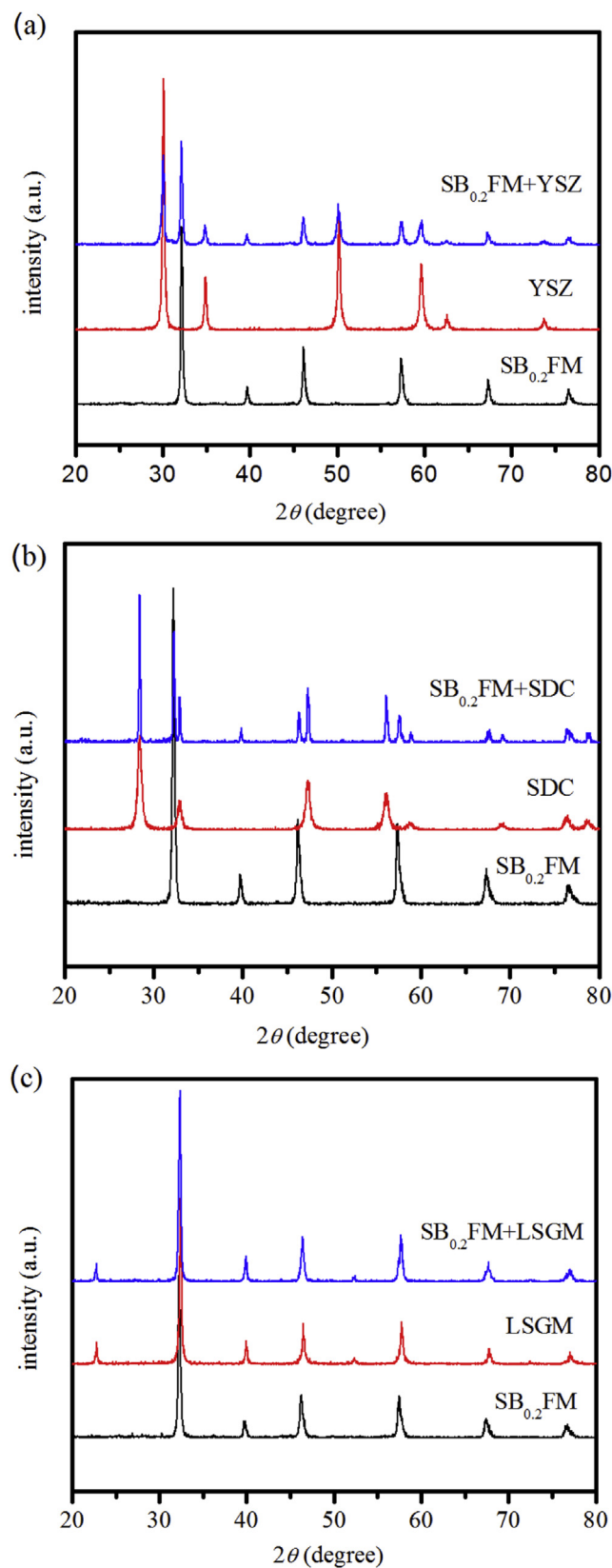


**Fig. 4.** XRD patterns of the of  $\text{SB}_{0.2}\text{FM}$  and electrolyte powders (50 wt% of each) after sintering at 800 °C for 48 h (a)  $\text{SB}_{0.2}\text{FM}$  and YSZ, (b)  $\text{SB}_{0.2}\text{FM}$  and SDC, (c)  $\text{SB}_{0.2}\text{FM}$  and LSGM.

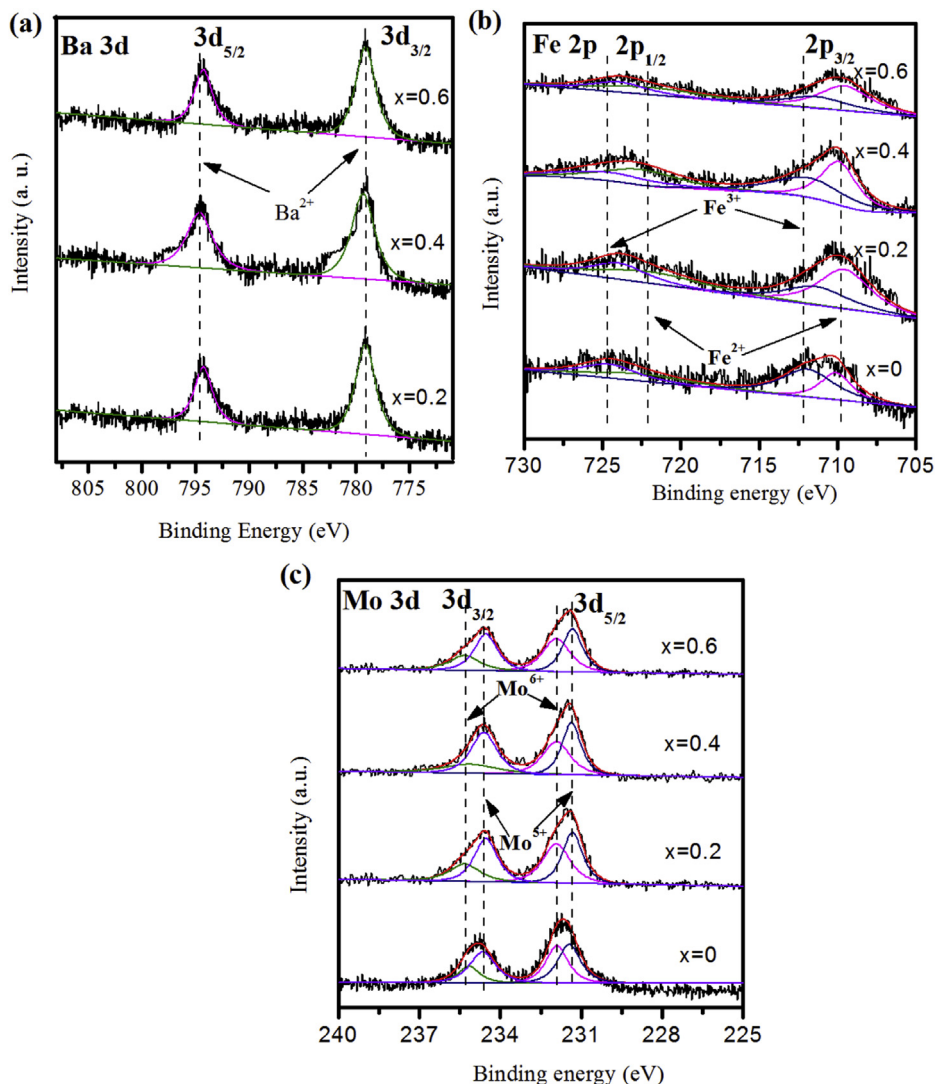


Fig. 5. XPS spectra at room temperature for SBFM samples (a) Ba 3d, (b) Fe 2p, (c) Mo 3d.

2p and Mo 3d spectra in SBFM samples at room temperature. The Ba 3d core-level XPS spectrum is shown in Fig. 5(a). Only one chemical state of Ba, i.e. the bivalent valence, was found in SBFM materials.

Fig. 5(b) shows the fitted XPS spectrum results of Fe 2p for SBFM samples. The spin-orbital splitting in the Fe 2p spectra exhibits double peaks of lower energy 2p<sub>3/2</sub> and higher energy 2p<sub>1/2</sub>. The peaks at 709.9 and 722.3 eV correspond to Fe<sup>2+</sup>(2p<sub>3/2</sub>) and Fe<sup>2+</sup>(2p<sub>1/2</sub>) respectively, whereas Fe<sup>3+</sup>(2p<sub>3/2</sub>) and Fe<sup>3+</sup>(2p<sub>1/2</sub>) are located at 711.2 and 724.8 eV, respectively [23]. The Mo 3d XPS spectra of SBFM samples are shown in Fig. 5(c). The characteristic peaks of Mo<sup>5+</sup> and Mo<sup>6+</sup> are 231.3 and 231.9 eV at 3d<sub>5/2</sub> and 234.6 and 235.1 eV at 3d<sub>3/2</sub> [24]. The XPS results clearly demonstrate the existence of Fe<sup>2+</sup>/Fe<sup>3+</sup> and Mo<sup>6+</sup>/Mo<sup>5+</sup> species in the SBFM samples. Moreover, no obvious change in the Fe 2p and Mo 3d profiles and insignificant influence on the Fe<sup>3+</sup> + Mo<sup>5+</sup> ↔ Fe<sup>2+</sup> + Mo<sup>6+</sup> process with the increasing Ba substitution level was observed.

#### 3.4. Characteristics of conductivities

For perovskite SBFM materials, the co-existence of electronic holes and oxygen vacancies makes the materials simultaneously

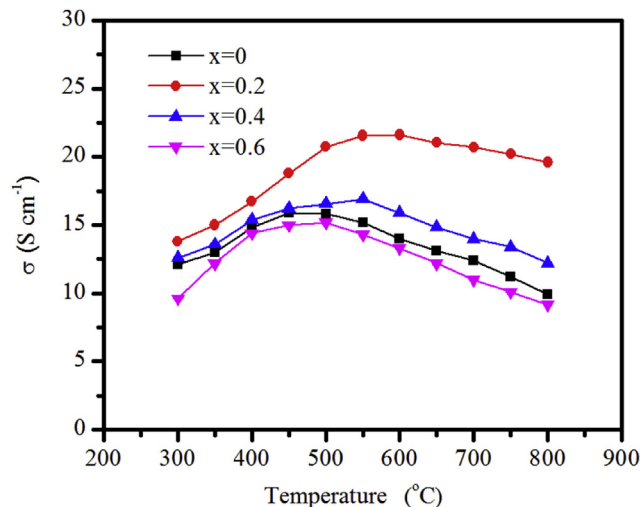
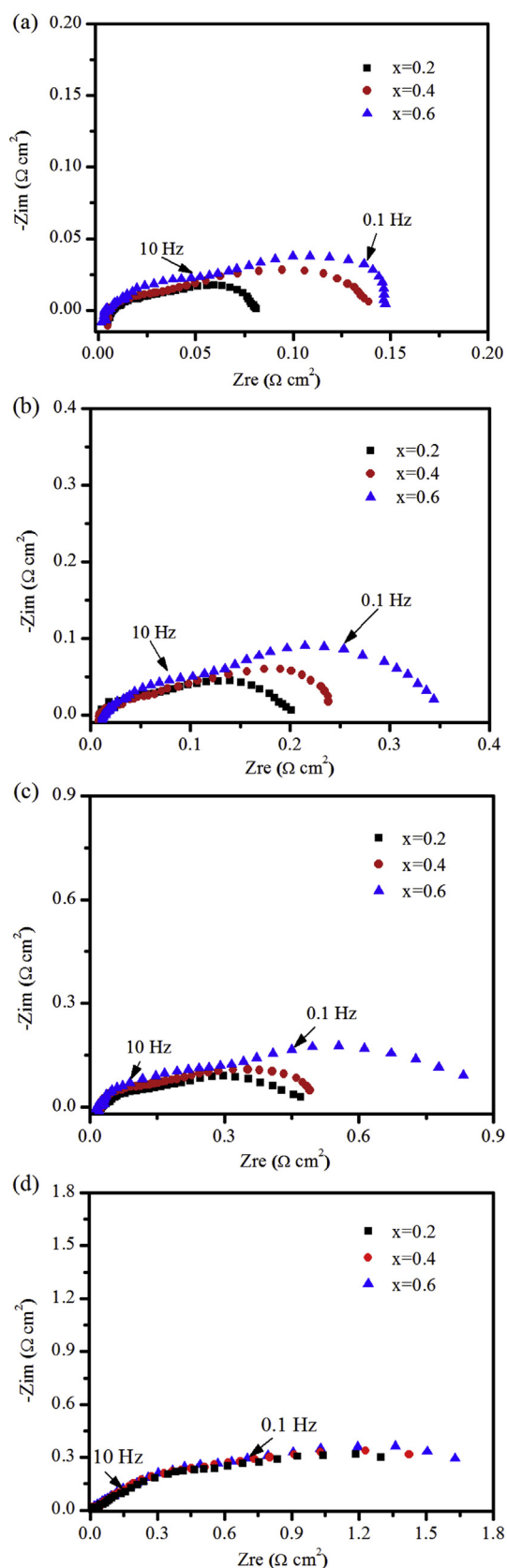


Fig. 6. Relation curves between conductivities of SBFM materials with different Ba-doping concentration and temperature.



**Fig. 7.** The EIS of the SBFM cathodes with different Ba-doping concentration measured in air at 800–650 °C (a) 800 °C, (b) 750 °C, (c) 700 °C, (d) 650 °C.

exhibit both electronic and ionic conductivity. The conductivities measured in this work can be mostly attributed to the electronic contribution as ionic conductivity is much lower than electronic conductivity. The temperature dependence of electronic conductivity ( $\sigma$ ) of SBFM samples in air from 300 °C to 800 °C is shown in Fig. 6. It is clear that the conductivity of the samples with different Ba-doping concentrations experiences at first an increase (p-type semi-conductivity) with temperature [12], reaching a maximum, and then a decrease when the temperature further increases. Furthermore, the total conductivity of SBFM decreases when the Ba concentration increases. When  $x = 0.2$ , the conductivity of  $\text{SB}_{0.2}\text{FM}$  sample reaches the maximum value of  $21.7 \text{ S cm}^{-1}$  at 550 °C, which is higher than that of SFM ( $\sigma = 15.9 \text{ S cm}^{-1}$ ) sample [14].

### 3.5. Polarization resistance

The area specific polarization resistance ( $R_p$ ) is an effective parameter to probe the catalytic activity of SOFC cathode for the ORR. The  $R_p$  of cathode was obtained by electrochemical impedance spectroscopy (EIS) measurements. The EIS for SBFM cathodes on YSZ electrolytes with an SDC interlayer was measured with a three-electrode system in air. The typical EIS can be fitted with the equivalent circuit  $LR_0(Q_H R_H)(Q_L R_L)$ . For comparison, the  $R_0$  was omitted in the Nyquist plots and the EIS of SBFM cathodes at 650–800 °C, as shown in Fig. 7. Compared with the  $R_p$  of SFM

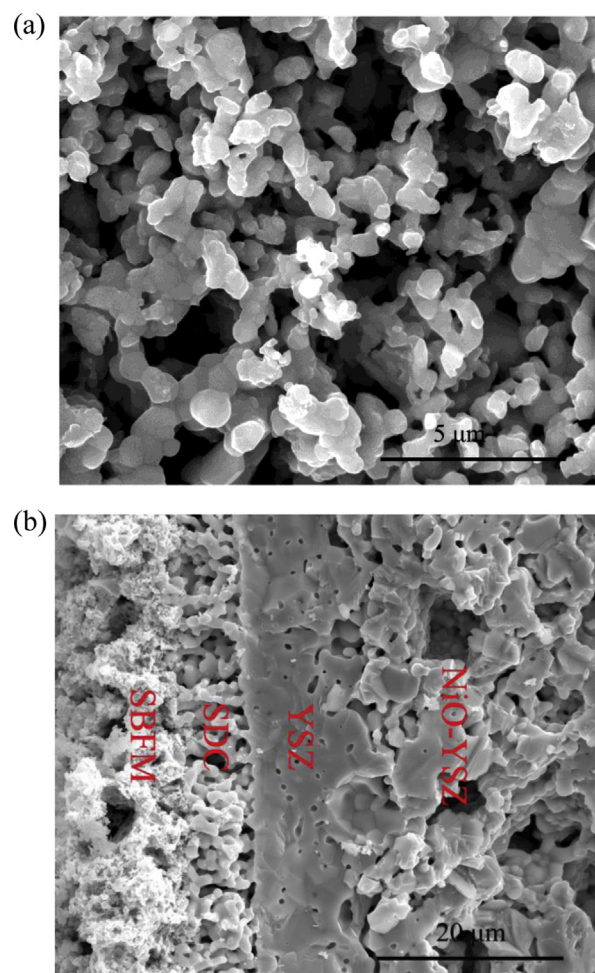


**Fig. 8.** The morphologies of the tested cell based on  $\text{SB}_{0.2}\text{FM}$  cathode (a) the surface of  $\text{SB}_{0.2}\text{FM}$  cathode, (b) the cross-section of the cell based on  $\text{SB}_{0.2}\text{FM}$  cathode.

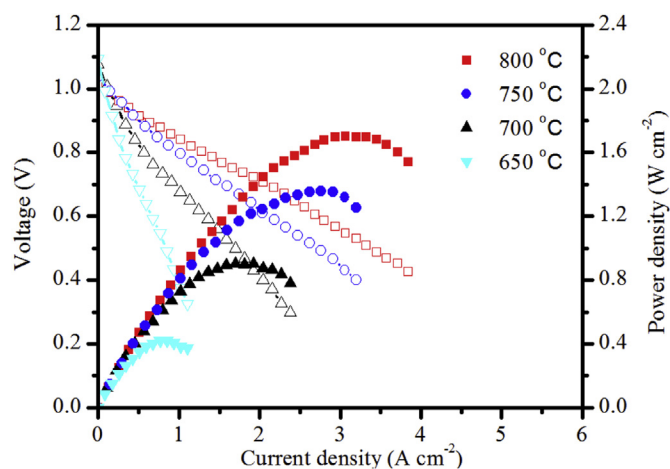


Fig. 9. The  $I$ - $V$  and  $I$ - $P$  curves of the single cell NiO-YSZ/YSZ/SDC/SB<sub>0.2</sub>FM in the temperature range 650–800 °C.

cathode [14], the  $R_p$  of SBFM cathodes apparently decreased at operating temperatures between 650 and 800 °C. Particularly, the SB<sub>0.2</sub>FM cathode exhibits the lowest  $R_p$ , which is only 0.19 and 0.43  $\Omega \text{ cm}^2$  at 750 and 700 °C, respectively, approximately 40% of the  $R_p$  of SFM cathode (0.42 and 0.92  $\Omega \text{ cm}^2$  at 750 and 700 °C, respectively). The enhancement of ORR rate and the decrease of the  $R_p$  of Ba-doped SBFM cathodes could be ascribed to the doping of Ba ions ( $\text{Ba}^{2+}$ ) which have larger radius than  $\text{Sr}^{2+}$  resulting in an expansion of the lattice spacing which is beneficial to oxygen ion movement.

### 3.6. Electrochemical properties and performance

For further evaluation of the electrochemical performance for SB<sub>0.2</sub>FM, we assembled anode supported NiO-YSZ/YSZ/SDC/SB<sub>0.2</sub>FM single cells based on the SB<sub>0.2</sub>FM cathode. Fig. 8 shows the surface of SB<sub>0.2</sub>FM cathode and the cross-section of the cell based on SB<sub>0.2</sub>FM cathode morphologies. The cathode surface maintained the porous network structure as shown in Fig. 8(a), which is favorable for oxygen transportation by providing rich reaction sites for electrons and oxygen ions transport, and the ORR in the electrode. Fig. 8(b) shows that the four layers, cathode, interlayer, electrolyte and anode, are firmly adhered to each other.

Fig. 9 reveals the  $I$ - $V$  and  $I$ - $P$  curves measured in the temperature range 650–800 °C. The power densities of single cells based on SB<sub>0.2</sub>FM cathodes were 0.41, 0.87, 1.30 and 1.63  $\text{W cm}^{-2}$  at 650, 700, 750 and 800 °C, respectively. All these results confirmed that SBFM electrodes are promising cathodes of IT-SOFCs due to their excellent electrochemical performance.

## 4. Conclusions

$\text{Sr}_{2-x}\text{Ba}_x\text{Fe}_{1.5}\text{Mo}_{0.5}\text{O}_{6-\delta}$  ( $x = 0.2, 0.4, 0.6$ ) (SBFM) materials have been successfully prepared using a sol-gel combustion method

and applied here as the cathodes for IT-SOFCs. XRD studies confirmed that SBFM consists of a pure perovskite structure. However impure phases could be observed in the samples when the Ba-doping concentration at high levels ( $x = 0.8$  and 1). The perovskite lattice expands with increasing Ba substitution in SBFM samples. In addition, the TECs of SBFM materials also increase with Ba doping. The XPS results show that Ba doping at the A-site in the perovskite barely changed the existence of  $\text{Fe}^{2+}/\text{Fe}^{3+}$  and  $\text{Mo}^{6+}/\text{Mo}^{5+}$  species within the SBFM samples. Moreover, in the three SBFM materials, the SB<sub>0.2</sub>FM cathode exhibits the lowest  $R_p$ , which was only 40% of the SFM cathode. The power densities of single cells with SB<sub>0.2</sub>FM cathodes are 1.30 and 1.63  $\text{W cm}^{-2}$  at 750 and 800 °C, respectively. These results indicate that the SBFM oxides are promising cathode materials for IT-SOFCs.

## Acknowledgments

This work is financial supported by National Natural Science Foundation of China (Grant Nos. 21006015 and 21070623) and is also supported by the Foundation of Beijing Key Laboratory for Chemical Power Source and Green Catalysis, contract No. 2013CX02031.

## References

- [1] S.D. Park, J.M. Vohs, R.J. Gorte, *Nature* 404 (2000) 265–267.
- [2] B.C.H. Steele, A. Heinzel, *Nature* 414 (2001) 345–352.
- [3] E.P. Murray, T. Tsai, S.A. Barnett, *Nature* 400 (1999) 649–651.
- [4] J.M. Vohs, R.J. Gorte, *Adv. Mater.* 21 (2009) 943–956.
- [5] Z.P. Shao, S.M. Haile, *Nature* 431 (2004) 170–173.
- [6] N.P. Brandon, S. Skinner, B.C.H. Steele, *Annu. Rev. Mater. Res.* 33 (2003) 183–213.
- [7] Y. Jiang, A.V. Virkar, *J. Electrochem. Soc.* 148 (2001) A706–A709.
- [8] A.J. Jacobson, *Chem. Mater.* 22 (2010) 660–674.
- [9] A. Chronos, B. Yildiz, A. Tarancon, D. Parfitt, J.A. Kilner, *Energy Environ. Sci.* 4 (2011) 2774–2789.
- [10] G.L. Xiao, Q. Liu, F. Zhao, L. Zhang, C.R. Xia, F.L. Chen, *J. Electrochem. Soc.* 158 (2011) B455–B460.
- [11] Q. Liu, D.E. Bugaris, G.L. Xiao, M. Chmara, S.G. Ma, H.-C.Z. Loye, M.D. Amiridis, F.L. Chen, *J. Power Sources* 196 (2011) 9148–9153.
- [12] Q. Liu, X.H. Dong, G.L. Xiao, F. Zhao, F.L. Chen, *Adv. Mater.* 22 (2010) 5478–5482.
- [13] X. Pan, Z.B. Wang, B.B. He, S.R. Wang, X.J. Wu, C.R. Xia, *Int. J. Hydrogen Energy* 38 (2013) 4108–4115.
- [14] N.N. Dai, J. Feng, Z.H. Wang, T.Z. Jiang, W. Sun, J.S. Qiao, K.N. Sun, *J. Mater. Chem. A* 1 (2013) 14147–14153.
- [15] X. Zhu, H. Wang, W.S. Yang, *Chem. Commun.* (2004) 1130–1131.
- [16] N.N. Dai, Z.L. Lou, Z.H. Wang, X.X. Liu, Y.M. Yan, J.S. Qiao, T.Z. Jiang, K.N. Sun, *J. Power Sources* 243 (2013) 766–772.
- [17] N.N. Dai, Z.H. Wang, Z.L. Lou, Y.M. Yan, J.S. Qiao, J. Peng, K.N. Sun, *J. Power Sources* 217 (2012) 519–523.
- [18] Q. Fu, K.N. Sun, N.Q. Zhang, S.R. Le, X.D. Zhu, J.H. Piao, *J. Solid State Electrochem.* 13 (2009) 455–467.
- [19] X.L. Zhou, K.N. Sun, J. Gao, S.R. Le, N.Q. Zhang, P. Wang, *J. Power Sources* 191 (2009) 528–533.
- [20] Y. Teraoka, M. Yoshimatsu, N. Yamazoe, T. Seiyama, *Chem. Lett.* 6 (1984) 893–896.
- [21] H. Liu, X. Zhu, M. Cheng, Y. Cong, W. Yang, *Chem. Commun.* 47 (2011) 2378–2380.
- [22] X.B. Li, H.Y. Wang, H.X. Gu, J. Wang, W.J. Zhang, T.G. Wang, *Sci. Sinter.* 42 (2010) 153–159.
- [23] A. Velazquez-Palenzuela, L. Zhang, L.C. Wang, P.L. Cabot, E. Brillias, K. Tsay, J.J. Zhang, *J. Phys. Chem. C* 115 (2011) 12929–12940.
- [24] L.L. Zhang, Q.J. Zhou, Q. He, T.M. He, *J. Power Sources* 195 (2010) 6356–6366.